J Ther Eng, Vol. 9, No. 5, pp. 1140−1152, September, 2023

Journal of Thermal Engineering
Web page info: https://jten.yildiz.edu.tr
DOI: 10.18186/thermal.1370699

Journal of Thermal Engineering

Research Article

Parametric evaluation of solar integrated combined partial cooling supercritical CO_2 cycle and Organic Rankine Cycle using low global warming potential fluids

Yunis KHAN[1,*], Radhey Shyam MISHRA[1], Roshan RAMAN[2], Abdul Wahab HASHMI3

[1]*Department of Mechanical Engineering, Delhi Technological University, Delhi 110042, India*
[2]*Department of Mechanical Engineering, The NorthCap University, Gurugram, Haryana, 122017, India*
[3]*Department of Mechanical Engineering, Advanced Manufacturing and Mechatronics Lab, MNIT Jaipur, 302017, India*

ARTICLE INFO

Article history
Received: 12 December 2021
Revised: 27 January 2022
Accepted: 03 Feburary 2022

Keywords:
Performance Analysis; Solar Power Tower; Organic Rankine Cycle; Partial Cooling Supercritical CO_2 Cycle; Low Global Warming Potential Fluids

ABSTRACT

In this study, the performance of the organic Rankine cycle combined with the partial cooling supercritical CO_2 cycle as the bottoming cycle for recovering the low grade heat powered by a solar power tower was evaluated. Ecofriendly fluids were taken into consideration. To simulate the model under consideration, a computer programme was created in engineering equation solver software. The impacts of solar radiation, concentration ratio, solar incidence angle, CO_2 turbine inlet temperature, heat exchanger effectiveness and main compressor inlet temperature were investigated. Based on working fluid R1224yd(Z), it was determined that the combined cycle's thermal efficiency, exergy efficiency, and power output improved from 35.16% to 55.43%, 37.73% to 59.42%, and 188 kW to 298.5 kW, respectively, as solar irradiation raised from 0.4 kW/m^2 to 0.95 kW/m^2. Lower the solar incidence angle and higher the concentration ratio can enhance the combined system's performance. Amongst the working fluids that were taken into account, R1224yd(Z) was suggested as having superior performance.

Cite this article as: Khan Y, Mishra RS, Raman R, Hashmi AW. Parametric evaluation of solar integrated combined partial cooling supercritical CO_2 cycle and Organic Rankine Cycle using low global warming potential fluids. J Ther Eng 2023;9(5):1140−1152.

INTRODUCTION

By 2030, the global energy demand will have increased by at least 50%. Production of carbon-free energy is necessary to ensure the security of the future [1]. The outstanding concentration solar power (CSP) system can meet the demand for safe and reliable electricity. Because of its high temperature generation, leading to in improved cycle efficiency, CSP systems are currently receiving significant interest in the power generation industry [2]. Consequently, the system's activity continuing past the critical stage, the minimum pressure of the supercritical carbon dioxide (sCO_2) Brayton cycle is higher (roughly 7.4 MPa) than any existed steam Rankine system (SRC) or gas Brayton cycle, making it a promising technology to produce electricity from such sources of high temperature [3]. The sCO_2

*Corresponding author.
*E-mail address: yuniskhan21@gmail.com

This paper was recommended for publication in revised form by Regional Editor Jovana Radulovic

Published by Yıldız Technical University Press, İstanbul, Turkey

is a good option because it is inexpensive, non-corrosive, non-flammable, non-toxic, and chemically stable. The operating fluid of a supercritical Brayton cycle (SBC) stays supercritical throughout the cycle and undergoes compression with a compressor rather than a pump, which is the key distinction between an SBC and an organic Rankine cycle (ORC) or steam Rankine technology. Since sCO_2 has a high fluid density, extremely compact turbo-machinery designs are possible, which makes them particularly attractive for waste heat recovery uses inside of automobiles. Recently, transcritical and supercritical configuration of the CO_2 based cycle are using for the high temperature. Also it has drawn a lot of attention due to much effectiveness of turbine and heat exchangers [4].

The combination of the thermal cycles performed efficiently than the fundamental thermal cycle. This cycle performed better when combined with a bottoming cycle like ORC to recover waste as opposed to a simple sCO_2 cycle. These combined cycles improved in safety, sustainability, and environmental sensitivity when heated by solar energy. To fully corroborate this claim, Al-Sulaiman [5] carried out a combination research of SRC and ORC operated by a solar parabolic trough collector (SPTC). They were successful in achieving a combined cycle thermal efficiency of 26% using R134a. Khatoon and Kim [6] investigated the combined recompression sCO_2 cycle and transcritical CO_2 cycle operated by solar power tower. They argued that an integrated cycle system was far better at converting power than just one power cycle. In a parametric analysis of sCO_2 for engines with internal combustion, Song et al. [7] combined it with the ORC. They found that while a cycle alone could provide 1170 kW of maximum power, adding an ORC generated an additional 250 kW of power.

A number of experiments were conducted to choose the ORC system's working fluids in addition to the solar-driven combined cycle. For example, Khan and Mishra [8] employed the ORC and an SPT-operated coupled CO_2 cycle. They discovered that adding the ORC as a bottoming cycle boosted energy efficiency and output power by 4.51% and 4.52%, respectively at DNI of 0.95 kW/m^2. Out of all the working fluids they examined, R227ea was suggested as having the best performance. Additionally, Khan and Mishra [9] did an energy evaluation of the SPTC powered sCO_2 cycle (partial heating) coupled with the ORC for waste heat recovery. They looked into six working fluids for ORC performance testing. According to the researchers, ORC boosted the basic sCO_2 (partial heating) system's energy efficiency by 4.47 percent. Using ORC as bottoming cycle, Singh and Mishra [10] have examined a SPTC-driven simple recuperated sCO_2 cycle. In another study, R245fa, R1234ze R134a, R407C and R1234yf were also investigated for temperature bottoming ORC. The SPTC driven partial heating sCO_2 cycle was partnered with the ORC With 78.07% and 43.49%, respectively, they found that the R407c combination cycle has the highest exergetic and energy efficiency. A study of the solar desalination system in 4E was done by Yanbolagh et al. [11]. The system showed the most favorable outcomes in regard to exergoeconomic, enviro-economic, and energy payback times. Finally, according to environmental research, the sun emits 6342, 48.169, and 18.46 kg of CO_2 and SO_2 each year.

Fluids with a high GWP and ODP (ozone depletion potential) such as chlorofluorocarbons, have been left out of the analysis. The ODP could only have a value that was less than one. Due to restrictions put in place by organizations like the European Union, the GWP was capped at less than 150 [12]. Just a few investigations have used zero ODP functioning fluids and ultra low GWP hydro fluoro olefin working fluids in the ORC to satisfy these specifications, such as Khan and Mishra's [2] investigation of eight such fluids. They came to an agreement that HFO working fluids outperformed HFC working fluid R134a in terms of thermal and environmental performance. The best working fluid was suggested as R1336mzz(Z). Using eight HFO low GWP working fluids, including R1233zd(E), R1224yd(Z), R1336mzz (Z), R1243zf, R1234ze(Z), R1225ye(Z), R1234yf, R1234ze(E) . Khan and Mishra [13] explored SPT-driven combined sCO_2 cycle and modified ORC. They found that R1243zf fluid had the best thermal and environmental performance. A model of solar-powered ORC with vapour compression refrigeration that uses R227ea, R236fa, R245fa, R1234ze, and R134a as working fluids was proposed by Khan and Mishra [14]. They found that R134a and R227ea are better refrigerants for cooling and generating electricity. In addition to the SRC and the ORC, the gas turbine cycle was also studied by Kose, Koc, and Yagli [15]. They investigate the thermodynamic effects of acetone, R113, R245fa, R152a, R141b and R365mfc. Based on R245fa, it was determined that the ORC's maximum net exergy and energy efficiency and net power were 22.6 percent, 64.76 percent, and 780.35 kW, respectively.

The literature review revealed that there were surprisingly few investigations on the solar integrated combination supercritical CO_2 cycle and the ORC employing extremely low GWP fluids. Additionally, it was noted that ORC was not done in conjunction with the SPT operated Partial Cooling sCO_2 (PCSCO2) cycle. This research purpose to bridge this gap by investigating the functioning of the partial cooling sCO_2 cycle operated with SPT and low GWP operating fluids in a bottoming ORC system. In other words, the innovation of this study is shown by the inclusion of the SPT system to the PCSCO2 cycle and using the waste heat the ORC was used. The major goal of the current study is to simultaneously choose the working fluids for an ORC system for recovering the wasted heat and to look at how system factors affect combined cycle performance. Performance criteria included exergy efficiency, energy efficiency, and power output. The effectiveness of heat exchanger-2 was studied, along with the effects of system factors like sun irradiation, concentration ratio, solar incidence angle, inlet temperature of sCO_2 turbine, and

main compressor. The EES software [16] is taken to create the programming equations for the system simulation.

System Description

Three sub systems were considered in this current systems, the first of which is a solar power system, the second of which is a partial cooling sCO_2 (PCSCO2) cycle, and the third of which is an ORC to recover low grade heat. Similar to the recompression cycle, the PCSCO2 cycle also uses a compressor and cooler, as seen in Figure 1. The amount of effort needed throughout the compression process is reduced by intercooling between various compressions steps [17]. It also performs more efficiently than the recompression arrangement at high inlet temperature of turbine. Furthermore, it is more resistant to variations in the pressure ratio cycle. This cycle is appropriate for warming since its pressure ratio is often higher than the recompression cycle [18]. These benefits of the partial cooling cycle have been taken into account when conducting the present study's additional investigation of this cycle.

The SPT system circulates the heat transfer fluid (HTF), which is molten salt, which powers the topmost PCSCO2 cycle. After getting heat from the HTF through HEX1 (heat exchanger-1) (state 4-5) sCO_2 stream goes to the sCO_2 turbine where it is expanded and work is obtained (state 5-6). Then it goes through the high temperature recuperator (HTR) where it heats the cold stream (state 6-7). The LTR (states 7-8) is the next device it passes through. With sCO_2 stream, some heat is still available. Through heat exchanger-2 (HEX2), the bottoming ORC makes use of the residual waste heat (states 8–11). The sCO2 stream enters the pre-compressor (C2) after going through the cooler and is compressed there to attain intermediate pressure (states 9–10). Following its division into two parts, the first part travels to the primary compressor (C1), and there it is compressed to the cycle's maximum pressure (state 10-1). Second stream goes to the recompressor (C3) from the intermediate pressure to the maximum cycle pressure (state 10-3). After the recompressor it mixes with cold stream coming out from the LTR before the HTR. Then total mass of cold stream enters in the HTR (state 3-4). Thus cycle repeats again and again. After getting the heat from the HEX2 organic fluid (R1234yf) enters in the organic turbine (OT) (state 5-6) where work is obtained. Expanded stream passes through the condenser (cond) where heat is rejected. Then it goes to the HEX2 (state 15-12) passing through the pump (state 14-15). Also ORC cycle repeats again and again.

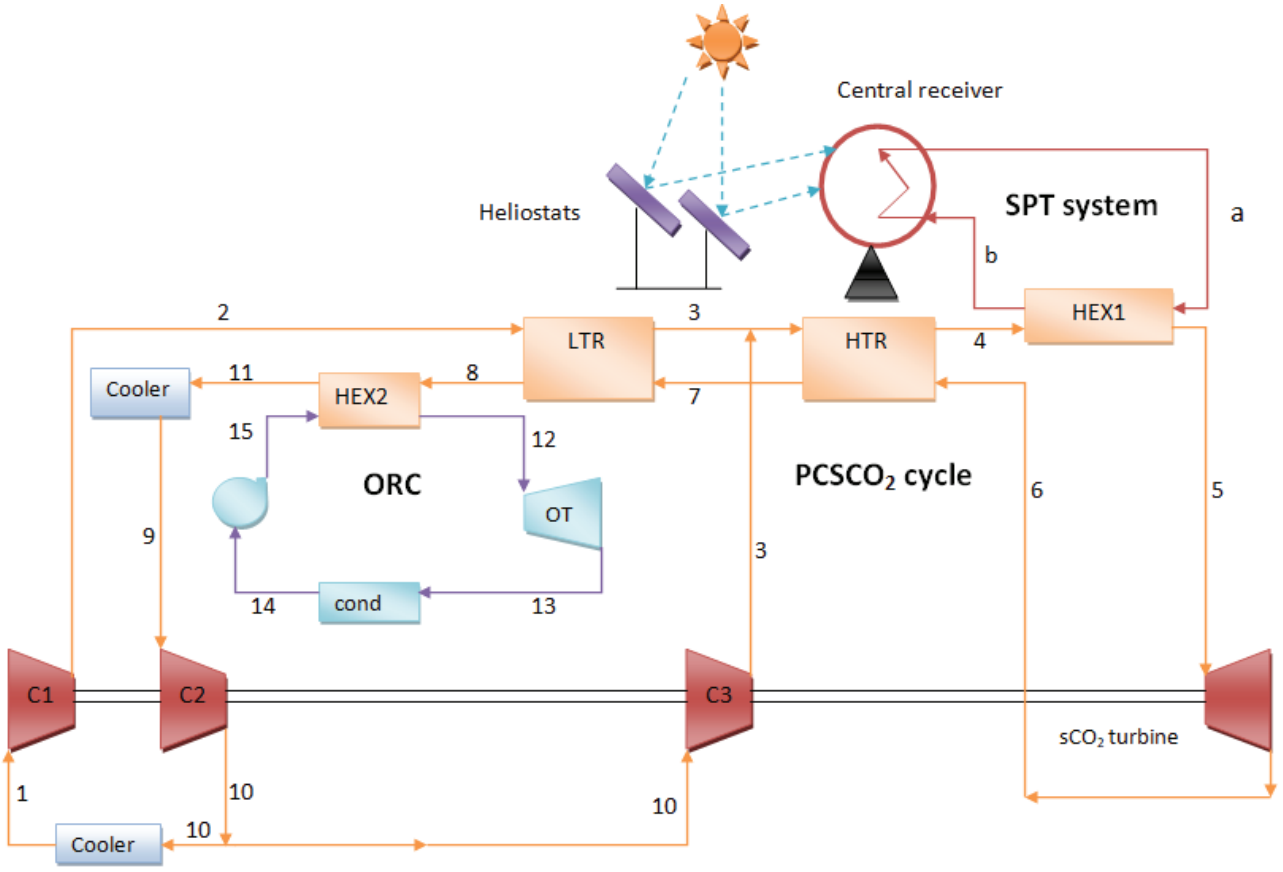

Figure 1. Combined partial cooling sCO_2 cycle and ORC driven by solar power tower.

THERMODYNAMIC ANALYSIS

Assumptions

For the simulation, certain presumptions have been made: (1) under conditions of steady state, each component is considered. (2) The pipe and components' pressure, friction, and heat loss are disregarded. (3) The compression and expansion processes are adiabatic. (4) The compressor and turbine isentropic efficiency is maintained. Table 1 contains the input values for the model simulation.

Table 1. Input variables for the combined system

SPT operational and geometric parameters	
Solar irradiation	850 W/m^2 [10]
Temperature of Sun	5800 K [5]
Coefficient of convective heat loss	10 W/m^2/K [19]
Solar multiple	2.8 [6]
Temperature difference initial	15 K [6]
Heliostat efficiency	58.71% [19]
Number of heliostat	141 [19]
Heliostat's total mirror area	9.04 x 7.89 m^2 [6]
Concentration ratio	900 [19]
Thermal emittance	0.85 [19]
Convective heat loss factor	1 [19]
Solar receiver's temperature approach	423.15 K [19]
Tower height	74.62 m [20]
Absorptance	0.95 [19]
View factor	0.8 [19]
Input data for combined cycle	
sCO_2 inlet temperature	800 °C [18]
Compressor inlet temperature	32 °C [21]
sCO_2 turbine inlet pressure	25 MPa [18]
Compressor isentropic efficiency	85% [21]
ORC pump's isentropic efficiency	70% [22]
Heat exchanger/recuperator effectiveness	95% [18]
Maximum pressure of ORC	3 MPa [2]
Mass flow rate of sCO_2	1.9 kg/s
ORC turbine's Isentropic efficiency	80% [7]
sCO_2 turbine isentropic efficiency	88% [21]
Minimum pressure of topping cycle	7.5 MPa [2]

Mathematical Modeling

The thermal modelling of the suggested system, on the basis of the presumptions in the preceding part, is presented in this section. In the first mathematical modeling of the SPT, Khatoon and Kim's earlier research [6] was used as a source.

Solar heat incidence on the heliostats is expressed as;

$$\dot{Q}_{solar} = DNI \cdot A_h \cdot N_h \quad (1)$$

Where, A_h heliostat area (m^2) and DNI is the irradiation incidence on heliostat, and N_h is heliostats number. However, actual amount of solar heat received by the heliostats are given as;

$$\dot{Q}_h = \dot{Q}_{solar} \cdot \eta_h \quad (2)$$

where the heliostats' efficiency is given by η_h. The resulting heat moves towards the solar receiver, where it conventionally combines with the heat transfer medium. The atmosphere does, however, lose some of the heat. As a result, the following formula is used to determine how much heat is obtainable through the solar centre receiver:

$$\dot{Q}_r = \dot{Q}_h \cdot \eta_r = \dot{Q}_h - \dot{Q}_{loss,r} \quad (3)$$

Where, η_r is the energy efficiency of receiver, is explained as;

$$\eta_r = \alpha - \frac{\zeta \cdot f_{view} \cdot \sigma \cdot T_R^4 + h_{conv} \cdot f_{conv} \cdot (T_R - T_{air})}{DNI \cdot \eta_h \cdot CR} \quad (4)$$

Where, T_R is the temperature of solar receiver surface. Concentrated ratio is given by CR while solar emittance by ζ.. It is expressed as;

$$T_R = T_1 + \delta T_R \quad (5)$$

Where, δT_R and T_1 are the approach temperatures of solar receiver and turbine's inlet temperature respectively. Solar receiver and the heliostat field's operating and geometric parameters are given in Table 1.Exergy destruction for each component can be evaluated as [22];

$$\sum \left(1 - \frac{T_0}{T_Q}\right) \dot{Q}_J - \dot{W}_{c.v} + \sum(\dot{m}_i E_i) - \sum(\dot{m}_e E_e) = \dot{ED} \quad (6)$$

Where, $\dot{ED}$ refers to rate of exergy destruction. The combined system is determined by the solar exergy inflow by Petela's formula [23];

$$\dot{E}_{solar} = \dot{Q}_{solar} \cdot \left[1 + \frac{1}{3}\left(\frac{T_0}{T_{su}}\right)^4 - \frac{4}{3}\left(\frac{T_0}{T_{su}}\right)\right] \quad (7)$$

Where, T_0 and T_{su} are the reference and sun temperature (5800 K) respectively. Further, with HTF receiver useful exergy can be expressed as;

$$\dot{E}_r = \dot{m}_{ms} \cdot Cp_{ms} \cdot \left[(T_b - T_a) - \left(T_0 \cdot ln\frac{T_b}{T_a}\right)\right] \quad (8)$$

In addition, the hour angle (ω) is calculated using local apparent time (LAT), It is created by adding the two

adjustments to the time that was determined by the clock. The following is the LAT expression [24]:

$$LAT = ST+4(\text{longitude of ST- location of longitude}) + (\text{Correction time equation}) \quad (9)$$

Where, standard time is ST.

The first modification is due to a discrepancy between a location's longitude and the meridian that ST is based on. In the first adjustment, the eastern and western hemispheres, respectively, are represented by the negative and positive signs. There has also been a correction magnitude of 4 minutes imposed for each degree of longitude variation. The second adjustment, the equation of correction time, is based on experimental data [24] and is necessary because the earth's orbit and rotational speed exhibit minute variations. The empirical relationship for the correction time equation can now be represented as [24, 28]:

$$E=229.18(0.000075+0.001868\cos B-0.032077\sin B-0.014615\cos 2B-0.04089\sin 2B) \quad (10)$$

$$B= (n-1)\ 360/365 \quad (11)$$

Where, years days is n.

The system's chemical exergy is continually constant. Absolute exergy due to physical condition at the jth location is defined as [5], after neglecting energy related to velocity and height.

$$E_j = (h_j - h_0) - T_0(h_j - s_0) \quad (12)$$

The heat balancing equation in HX1determines the amount of heat received from the SPT field.

$$\dot{Q}_r = \dot{Q}_{HX1} = \dot{m}_{ms} \cdot Cp_{ms} \cdot (h_b - h_a) = \dot{m}_{SCO2} \cdot (h_5 - h_4) \quad (13)$$

Output power from the main turbine is expressed as;

$$\dot{W}_{sCO2\ turbine} = \dot{m}_{SCO2} \cdot (h_1 - h_{2s}) \cdot \eta_{sCO2\ turbine} \quad (14)$$

Where, $\eta_{sCO2\ turbine}$ is the turbine isentropic efficiency, and h_{2s} is the enthalpy at the main turbine's outlet when expansions was achieved isentropically.

Heat exchange in HTR [29];

$$\dot{Q}_{HTR} = \dot{m}_{sCO2} \cdot (4_4 - h_3) = \dot{m}_{sCO2} \cdot (h_6 - h_7) \quad (15)$$

Where, $\dot{m}_{sCO2}$ is the CO_2 mass flow rate. The HTR effectiveness with the same mass flow rate on the hot and cold sides is calculated as;

$$\varepsilon_{HTR} = \frac{T_4 - T_3}{T_6 - T_3} \quad (16)$$

The main compressor (C1), pre-compressor (C2), recompressor (C3) power input are defined as;

$$\dot{W}_{C1} = \frac{x \cdot \dot{m}_{sCO2} \cdot (h_{4s} - h_3)}{\eta_{C1}} \quad (17)$$

$$\dot{W}_{C2} = \frac{\dot{m}_{sCO2} \cdot (h_{10s} - h_9)}{\eta_{C2}} \quad (18)$$

$$\dot{W}_{C3} = \frac{(1-x) \cdot \dot{m}_{sCO2} \cdot (h_{3s} - h_{10})}{\eta_{C3}} \quad (19)$$

Where, η_{C1}, η_{C2} and η_{C3} are the main, pre and re compressor's isentropic efficiencies respectively. The mass percentage of the sCO_2 stream that is sent to the main compressor is x. The heat balance and effectiveness formula are also used to define heat transfer in LTR.

$$\dot{Q}_{LTR} = x \cdot \dot{m}_{sCO2} \cdot (h_3 - h_2) = \dot{m}_{sCO2} \cdot (h_8 - h_7) \quad (20)$$

The effectiveness of LTR is calculated as;

$$\varepsilon_{LTR} = \frac{T_3 - T_2}{T_7 - T_2} \quad (21)$$

Heat rejection through the cooler has been calculated as;

$$\dot{Q}_{HEX2} = \dot{m}_{SCO2} \cdot (h_{11} - h_9) \quad (22)$$

ORC heat absorbed through the HEX2 can be expressed by;

$$\dot{Q}_{HEX2} = \dot{m}_{SCO2} \cdot (h_8 - h_{11}) = \dot{m}_{ORC} \cdot (h_{15} - h_{12}) \quad (23)$$

Where, $\dot{m}_{ORC}$ is working fluid mass flow rate flowing in the ORC.

The HEX2 effectiveness is calculated as;

$$\varepsilon_{LTR} = \frac{C_{ORC} \cdot (T_{12} - T_{15})}{C_{min} \cdot (T_8 - T_{15})} = \frac{C_{sCO2} \cdot (T_8 - T_{11})}{C_{min} \cdot (T_8 - T_{15})} \quad (24)$$

Where, C_{sCO2} and C_{ORC} are the heat capacities of sCO_2 and working fluid flowing in ORC respectively. C_{min} is the minimum heat capacities of two fluids.

Output power of the ORC turbine is calculated as;

$$\dot{W}_{OT} = \dot{m}_{ORC} \cdot (h_{12} - h_{13s}) \cdot \eta_{OT} \quad (25)$$

Where, η_{OT} is the of ORC turbine efficiency.

Condenser heat can be expressed as;

$$\dot{Q}_{cond} = \dot{m}_{ORC} \cdot (h_{13} - h_{14}) \quad (26)$$

The pump's ability to absorb power can be defined as;

$$\dot{W}_{pump} = \frac{\dot{m}_{ORC} \cdot (h_{15s} - h_{14})}{\eta_{pump}} \quad (27)$$

Where, η_{pump} is the pump isentropic efficiency.

The net power of each bottoming ORC is determined as;

$$\dot{W}_{net,ORC} = \dot{W}_{OT} - \dot{W}_{pump} \quad (28)$$

This section will also discuss the integrated system's exergy analysis. Exergy destruction and in all elements are evaluated by the exergy balancing equation [22] after presuming there is no heat loss in the unit.

The loss of energy in the cooler is neglected. Heat exchanger 1's exergy formula is written as;

$$\dot{m}_{sCO2} \cdot [(h_5 - h_4) - T_0(s_5 - s_4)] + \dot{m}_{ms} \cdot [(h_a - h_b) - T_0(s_a - s_b)] - \dot{E}D_{HEX1} = 0 \quad (29)$$

The exergy balancing equation for the primary turbine can be written as;

$$\dot{m}_{sCO2} \cdot [(h_5 - h_6) - T_0(s_5 - s_6)] - \dot{W}_{sCO2\,turbine} - \dot{E}D_{sCO2\,turbine} = 0 \quad (30)$$

For example, the HTR exergy equilibrium formula is;

$$\dot{m}_{sCO2} \cdot [(h_6 - h_7) - T_0(s_6 - s_7)] + \dot{m}_{sCO2} \cdot [(h_4 - h_3) - T_0(s_4 - s_3)] - \dot{E}D_{HTR} = 0 \quad (31)$$

Exergy balance equations for the main compressor (C1), pre-compressor (C2) and the recompressor (C3) respectively, are determined as;

$$x \cdot \dot{m}_{sCO2} \cdot [(h_{10} - h_1) - T_0(s_{10} - s_1)] + \dot{W}_{C1} - \dot{E}D_{C1} = 0 \quad (32)$$

$$\dot{m}_{sCO2} \cdot [(h_9 - h_{10}) - T_0(s_9 - s_{10})] + \dot{W}_{C2} - \dot{E}D_{C2} = 0 \quad (33)$$

$$(1 - x) \cdot \dot{m}_{sCO2} \cdot [(h_3 - h_{10}) - T_0(s_3 - s_{10})] + \dot{W}_{C3} - \dot{E}D_{C3} = 0 \quad (34)$$

The LTR exergy balance equation is as follows;

$$\dot{m}_{sCO2} \cdot [(h_3 - h_2) - T_0(s_3 - s_2)] + \dot{m}_{sCO2} \cdot [(h_7 - h_8) - T_0(s_7 - s_8)] - \dot{E}D_{LTR} = 0 \quad (35)$$

The following is the HEX2 exergy equilibrium calculation:

$$\dot{m}_{sCO2} \cdot [(h_8 - h_{11}) - T_0(s_8 - s_{11})] + \dot{m}_{ORC} \cdot [(h_{12} - h_{15}) - T_0(s_{12} - s_{15})] - \dot{E}D_{HEX2} = 0 \quad (36)$$

The OT exergy balance equation is as follows;

$$\dot{m}_{ORC} \cdot [(h_{12} - h_{13}) - T_0(s_{12} - s_{13})] - \dot{W}_{OT} - \dot{E}D_{OT} = 0 \quad (37)$$

The condenser exergy balance equation is as follows;

$$\dot{m}_{ORC} \cdot [(h_{13} - h_{14}) - T_0(s_{13} - s_{14})] - \dot{E}D_{cond} = 0 \quad (38)$$

The pump exergy balance equation is as follows;

$$\dot{m}_{sCO2} \cdot [(h_{15} - h_{14}) - T_0(s_{15} - s_{14})] + \dot{W}_{pump} - \dot{E}D_{pump} = 0 \quad (39)$$

Total exergy destruction can be calculated as;

$$\dot{E}D_{total} = \dot{E}D_{HEX1} + \dot{E}D_{sCO2\,turbine} + \dot{E}D_{HTR} + \dot{E}D_{C1} + \dot{E}D_{C2} + \dot{E}D_{C3} + \dot{E}D_{LTR} + \dot{E}D_{HEX2} + \dot{E}D_{OT} + \dot{E}D_{cond} + \dot{E}D_{pump} + \dot{E}D_{reciever} \quad (40)$$

On the basis of thermal modelling, the following list of mathematical relationships used to evaluate the SPT-driven combined cycle's performance;

The net power output is computed as follows:

$$\dot{W}_{net} = \dot{W}_{sCO2\,turbine} + \dot{W}_{OT} - \dot{W}_{C1} - \dot{W}_{C2} - \dot{W}_{C3} - \dot{W}_{pump} \quad (41)$$

A solar-powered system thermal efficiency is determined as follows:

$$\eta_{th} = \frac{\dot{W}_{net}}{\dot{Q}_{solar}} \quad (42)$$

The calculation of combined cycle exergy efficiency is [22];

$$\eta_{ex} = 1 - \frac{\dot{E}D_{total}}{\dot{E}_{solar}} = \frac{\dot{W}_{net}}{\dot{E}_{solar}} \quad (43)$$

Thermal efficiency can also be calculated by the relation [22];

$$\eta_{th} = \eta_{ex} \cdot \eta_{Carnot} \quad (44)$$

Working fluid selection

The thermal, financial, and environmental sustainability of the thermal power plant are significantly impacted by the working fluid selection. Molten (32 percent MgCl2 and 68 percent KCl) is used as HTF in the SPT system

Table 2. Fluids properties considered in this work [2]

Fluids	Weight (Kg/Kmole)	Tc (°C)	Type	Tb (°C)	Pc (MPa)	ODP	GWP	Lifetime (years)	Security group
R1336mzz(Z)	164.000	171.30	D	33.40	2.903	0	8.9	0.0602	A1
R1234yf	114.040	094.70	I	-30.00	4.597	0	<1	-	A2L
R1224yd(Z)	148.500	155.50	I	14.00	3.330	0	0.88	-	A1
R1225ye(Z)	130.500	106.50	I	-20.00	3.335	0	0.87	-	-
R1234ze(Z)	114.040	150.10	I	09.80	3.530	0	<10	-	
R1233zd(E)	130.500	165.50	I	18.32	3.570	0	1	-	A1
R1234ze(E)	114.043	109.40	D	-19.00	3.640	0	6	0.0250	A2L
R1243zf	096.050	104.44	D	-25.41	3.518	0	<1	-	A2

because it is the least expensive alternative for the SPT-operated sCO_2 cycle as opposed to solar salt and liquids sodium (Na). On the other hand, the ORC takes into account working fluids with extremely low GWP and 0 ODP while still taking into account European Union rules. The eight HFO working fluids, including R1233zd(E), R1224yd(Z), R1234ze(E), R1234yf, R1243zf, R1225ye(Z), R1336mzz(Z), and R1234ze(Z), are taken into consideration in this analysis. Table 2 lists the thermophysical and environmental characteristics where D and I denotes dry and isentropic respectively. The vapour pressure of a fluid at the temperature below which separate phases of gas and liquid are not present is known as the critical pressure (Pc). The greatest temperature at which a gas can be liquefied under pressure is known as the critical temperature (Tc). The temperature at which an atmospheric fluid boils is known as the boiling point (Tb). The safety category classification has two or three numerical values (such as B1 or A2L) for each working fluid. With or without a suffix letter, the first character and number denotes toxicity and flammability respectively. There are two levels of toxicity: Class A is the lowest level and Class B is the highest level. Currently four flammability groups: 1, 2L, 2, or 3, according to [25,30,31].

Verification of the Suggested Model

To ensure that the modeling equation is accurate, the current model must be verified. PCSCO2 cycle and ORC were independently validated under the identical baseline conditions as earlier investigations by Kulhanek and Dostal [26] and Song et al. [27]. Figure 2 illustrates validation of the PCSCO2 cycle's thermal efficiency with earlier research. It is clear that the present model's thermal efficiency pattern and turbine pressure ratio are very similar to earlier research. As shown in Table 3, ORC were validated with a prior study by Song et al. [27]. It discovered that the calculated results and those of earlier investigations were extremely similar.

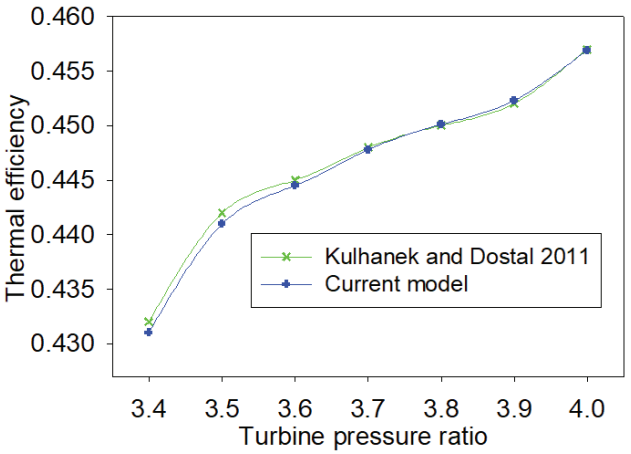

Figure 2. Validation of thermal efficiency of the $PCSCO_2$ cycle.

Table 3. ORC Validation

Working fluid	Thermal efficiency		Error estimated
	Song et al. [27]	Present system	
R245fa	11.4%	11.6%	-1.75%

RESULTS AND DISCUSSION

Direct Normal Irradiation Variation

The impact of LAT on the DNI is depicted in Figure 3. 30 minutes have been added to the DNI resolution. It noted that the study for Mumbai, India, has been done on two distinct dates, i.e., 15th April and December 15th . It was discovered that on April 15th the value of DNI was higher than on December 15th . As It may observed , the greatest DNI values for the 15th of April and December are approximately 0.705 kW/m^2 and 0.580 kW/m^2, respectively, at LAT(h)=1230, At LAT(h)=0730, the minimal results are, respectively, 0.145 kW/m^2 and 0.081 W/m^2 [24].

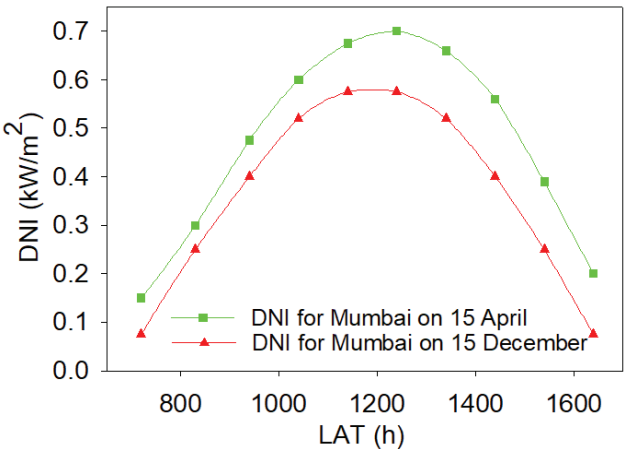

Figure 3. DNI variation with LAT.

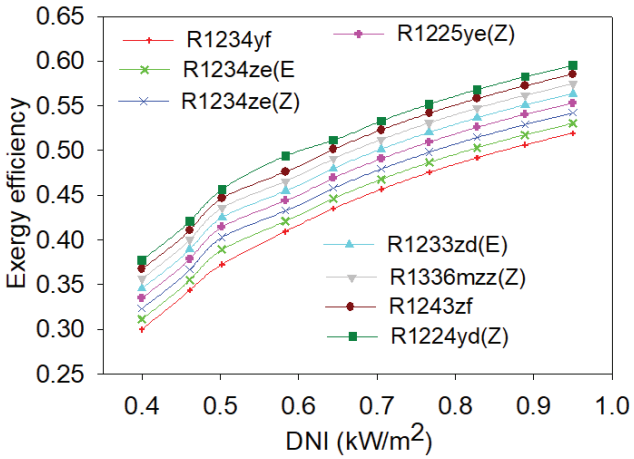

Figure 5. DNI effects on exergy efficiency.

Effects of Direct Normal Irradiation on System Performance

Since the present research focuses on solar energy, it is essential to look into how solar radiation or DNI affects system performance. Thermodynamic performance increased with DNI while all other variables stay constant. Due to the abundance of heliostats, sun radiation was efficiently used with them. Instead, as solar irradiation grew, receiver efficiency did as well; it enhanced the solar-powered system's performance. Thus, the DNI improved the performance of system. Among the various working fluids under consideration, R1224yd (Z) demonstrated the best thermal performance, followed by R1234yf, R1336mzz(Z) R1243zf , R1234ze(Z), R1234ze(E), R1233zd(E), and R1225ye(Z). Based on working fluid R1224yd(Z), the combined cycle's best thermal and exergy efficiency, and power rose from 35.16% to 55.43%, 37.73% to 59.42%, and 188 kW to 298.5 kW, respectively. As according to Figures 4-6, DNI enhanced from 0.4 to 0.95 kW/m^2.

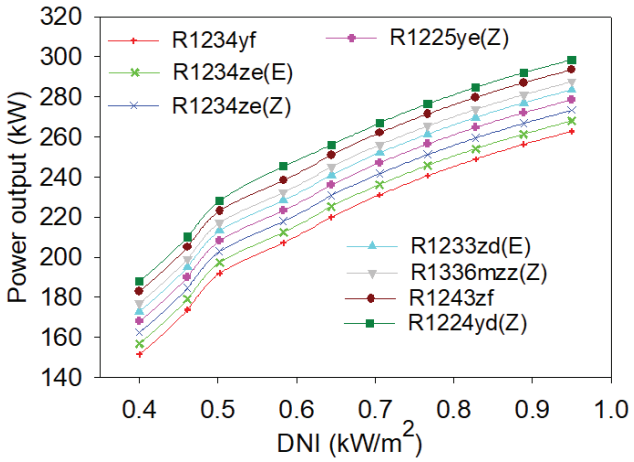

Figure 6. DNI effects on power output.

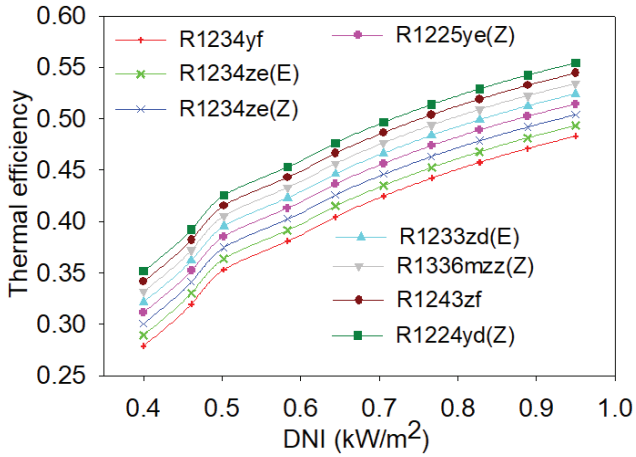

Figure 4. DNI effects on thermal efficiency.

System Performance Analysis with Concentration Ratio

This section must address the effect of the concentration ratio (CR). The receiver's efficiency grows with the concentration ratio, which explains this. Consequently, the solar-powered plant efficiency will improve with the ratio of concentration. Alternately, when the concentration ratio rises, the heliostats are able to capture more heat energy, increasing the pace at which work is produced. The result is thermal performance improvement. R1224yd(Z), one of the fluids that worked tested, produced the best outcomes. The working fluid R1224yd(Z) was employed as the CR rose from 200 to 1400. As a result, the thermal efficiency, exergy efficiency, and power output improved from 37.05% to 56.70%, 39.76% to 60.89%, and 148.2 kW to 347.7kW, respectively. However, R1234yf performed the least well out of the working fluids that were chosen. As seen in Figures 7-9, the performance of the other fluids lies in a range between these two fluids.

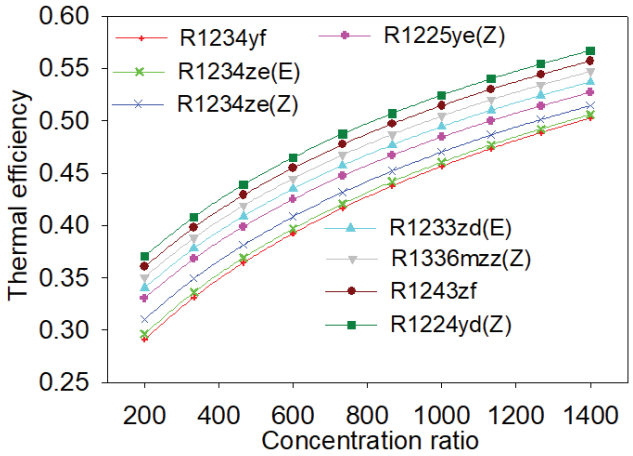

Figure 7. Effects of the concentration ratio on the thermal efficiency.

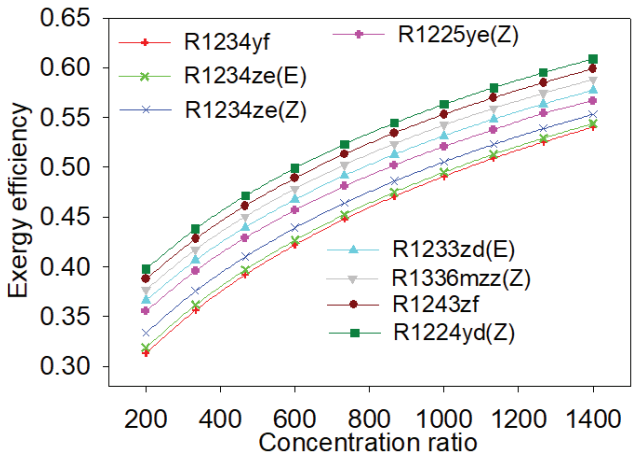

Figure 8. Effects of the concentration ratio on the exergy efficiency.

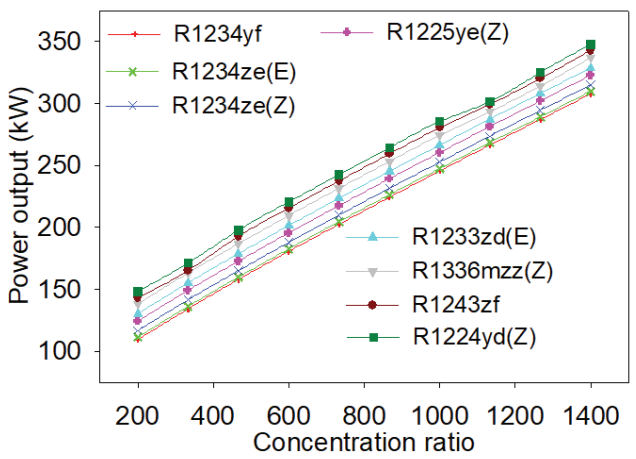

Figure 9. Concentration ratio effects power output.

Incidence Angle Effect on Performance of the Plant

It is also necessary to talk about the incidence angle because it significantly affects the solar system's performance. The solar power system is impacted by this. As the angle of solar incidence increased, the system's thermodynamic performance suffered. The exergetic efficiency, thermal efficiency, and solar efficiency all decline as the angle of incidence rises, reducing the performance of the solar-powered system. In contrast, beam irradiation dropped as incidence angle increased, which led to a decline in the system's optical efficiency. As a result, the receiver's efficiency drops. Owing to the R1224yd(Z) working fluid, as seen in Figures 10–12, when the incident angle grows from 3 degrees to 30 degrees, the thermal, exergy efficiency, and power output decrease from 58.29% to 56.84%, 62.22% to 60.66%, and 291.4 kW to 283.8 kW, respectively.

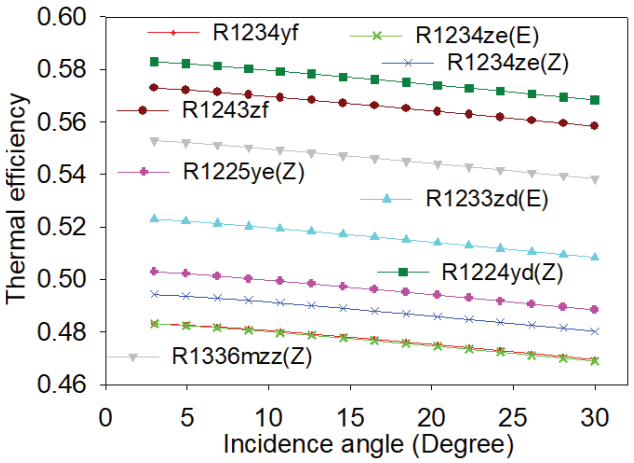

Figure 10. Variation in thermal efficiency with respect to angle of incidence.

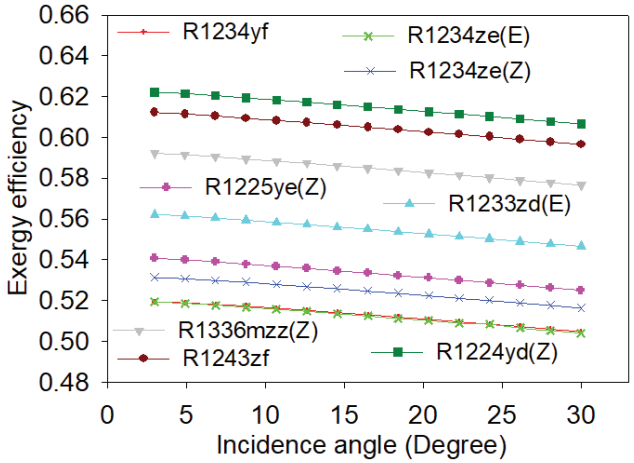

Figure 11. Variations in exergy efficiency with respect to angle of incidence.

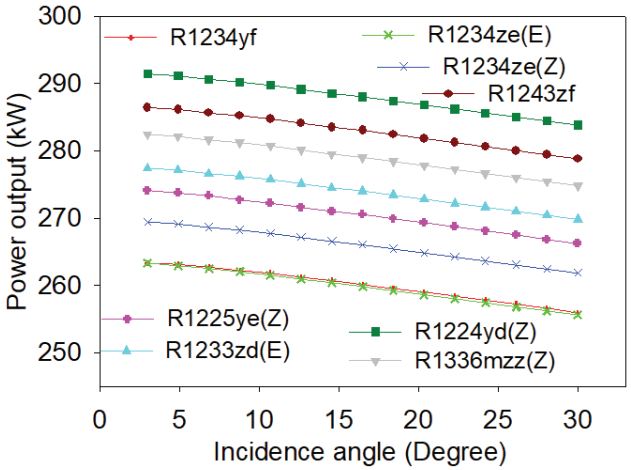

Figure 12. Power output variation with the incidence angle.

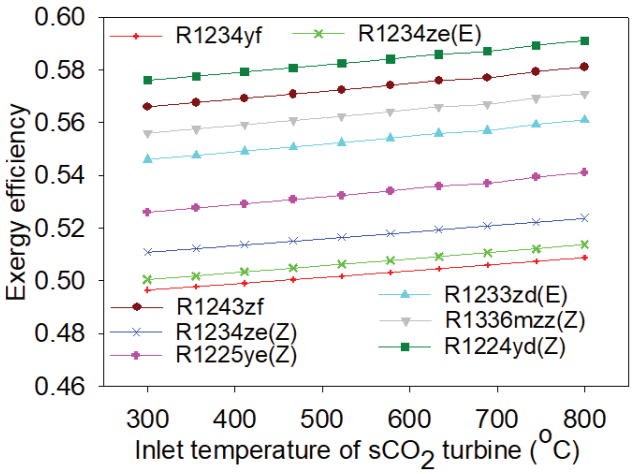

Figure 14. Exergy efficiency of a sCO_2 turbine varies with inlet temperature.

Effects of System Performance on sCO_2 Turbine Temperature at the Inlet

The first parameter that will be looked at is sCO_2 turbine temperature at the inlet. The system's thermodynamic performance rises as the turbine's inlet temperature does. As the temperature rises, the inlet enthalpy rises as well. Therefore, when the difference in enthalpies grows, power output also grows. As a result, thermal efficiency rises as inlet temperature of turbine does. Based on the R1224yd(Z) temperature increases from 300°C to 800°C as illustrated in Figures 13–15, the output power increases from 294.7 kW to 297.3 kW, the thermal efficiency changed from 39.76% to 60.89%, and the exergy efficiency rises from 57.60% to 59.10%.

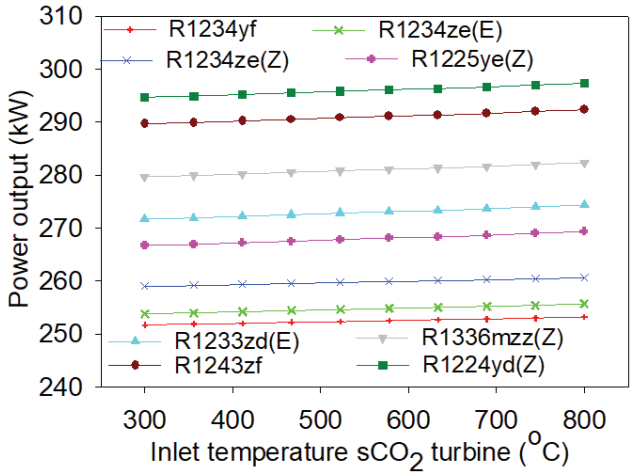

Figure 15. Effects of system power output on sCO_2 turbine temperature at the inlet.

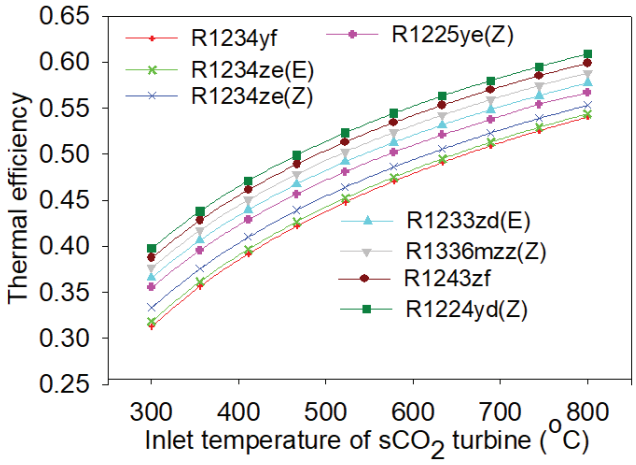

Figure 13. Effects of system thermal efficiency on sCO_2 turbine temperature at the inlet.

Effect of Main Compressor's Inlet Temperature on Performance of the System

The temperature of the main compressor inlet affects how well a combined cycle system works. The integrated cycle's thermal efficiency decreases as the inlet temperature of compressor rises. As the input temperature rises, the specific heat of the carbon dioxide rises. Deference in the enthalpy consequently rises, increasing the compression work. Consequently, the net output declines. Consequently, combined cycle performance suffers. As the main compressor temperature rises from 32°C to 38°C based on the working fluid R1224yd(Z), the thermal efficiency, exergy efficiency, and power output fall from 51.92% to 49.95%, 55.82% to 53.70%, and 280.7 kW to 269.9 kW, respectively. As seen in figures 16–18, working fluid R1234yf performs the least well compared to the other working fluids.

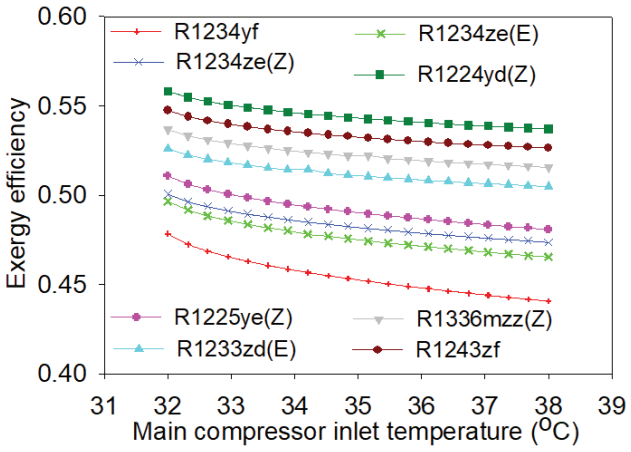

Figure 16. Exergy efficiency varies with inlet temperature at the main compressor.

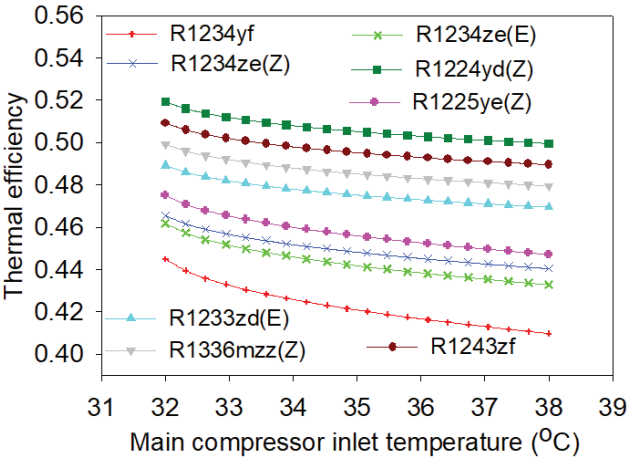

Figure 17. Exergy efficiency varies with inlet temperature at the main compressor.

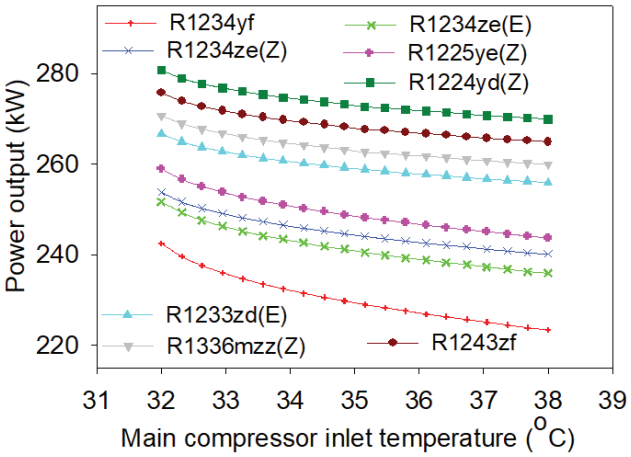

Figure 18. Power output vs. compressor temperature.

Effect of Heat Exchanger-2 Effectiveness on System Performance

Bottoming cycle performance completely depends on the heat exchanger, making it the most important parameter to be looked into. It serves as a bridge between the bottoming cycle and the topping sCO_2 cycle, making it a crucial part of the combined cycle. Consequently, great consideration must be given to the heat exchanger's design. With efficacy come advances in thermal efficiency and electricity production. The bottoming cycle produces more waste heat as effectiveness rises. Due to the fact that the growth of net work outpaces the addition of heat to the bottoming cycle combined power output and thermal efficiency rise. It has been found that the thermal efficiency is improving less quickly than its efficacy. This results from the combined impact of the bottoming cycle's heat addition. As demonstrated in Figure 19, as the effectiveness increases from 0.85 to 0.95 while maintaining other design parameters constant, thermal efficiency increases from 50.66% to 51.20%, and power output goes from 285.3 kW to 288.2 kW.

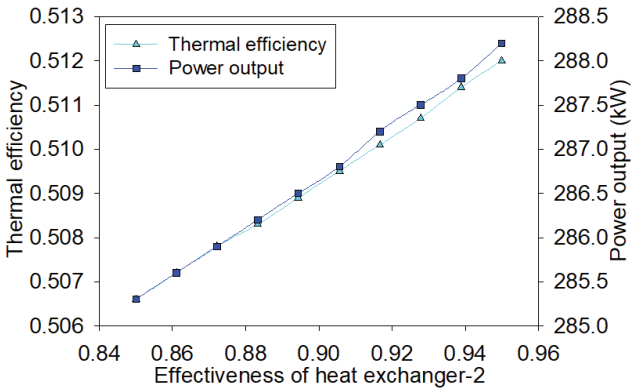

Figure 19. Effects of effectiveness of heat exchanger-2 thermal performance.

CONCLUSIONS

The findings that were drawn from present work are listed below.

- The efficiency of the heat exchanger-2, rapid increase in concentration ratio caused by the sCO_2 turbine's inlet temperature, and higher solar radiation all improved the combined system's performance. The compressor's inlet temperature and the solar incidence angle decreased it on the other side.
- Based on working fluid R1224yd(Z), highest output power, exergy and thermal efficiency rose from 188 kW to 298.5 kW, 37.73% to 59.42%, and 35.16% to 55.43%, respectively. DNI changed from 400 W/m^2 to 950 W/m^2.
- By reducing the solar incidence angle while raising the concentration ratio, combined cycle performance can be enhanced.

- The SPT needs to be properly developed in order to enhance the performance of the combined power cycle.
- Among various working fluids that were thought to have a low GWP, R1224yd(Z) was suggested as having a higher performance.
- It can be argued that the proposed power system is useful for producing clean energy. Due to the proposed combined power system's lack of environmental emissions, it is a realistic power production system with no effect on ozone depletion or global warming.

NOMENCLATURE

$\dot{Q}_h$	Heliostat field heat (kW)
A_h	Area of heliostat (m^2)
DNI	Direct normal irradiation (W/m^2)
f_{view}	Receiver's view factor
$\dot{E}_{solar}$	Solar exergy (kW)
$\dot{E}$	Exergy rate (kW)
Cp	Specific heat (kJ/kg-K)
N_h	Number of heliostat
$\dot{Q}_{loss,r}$	Receiver heat loss (kW)
h	Specific enthalpy (kJ/kg)
$\dot{Q}_{solar}$	Solar heat (kW)
$\dot{W}$	Power (kW)
T	Temperature (K)
sCO_2	Supercritical carbon dioxide
$\dot{E}D$	Exergy destruction rate (kW)
$\dot{Q}$	Heat rate in (kW)
SPT	Solar power tower
$\dot{m}$	Mass flow rate (kg/s)
η_h	Heliostat efficiency
η_{th}	Thermal efficiency
s	Specific entropy (kJ/kg-K)
x	Fraction of mass of sCO_2
η_{ex}	Exergy efficiency
η_r	Receiver thermal efficiency
$\dot{Q}_r$	Central receiver heat (kW)

Abbreviations

C1	Main Compressor
C2	Pre-compressor
Cond	condenser
HTR	High temperature recuperator
C3	Recompressor
CR	Concentration ratio
HEX2	Heat exchanger-2
ORC	Organic Rankine cycle
$PCSCO_2$	Partial cooling sCO_2 cycle
LTR	Low temperature recuperator
HEX1	Heat exchanger-1
OT	ORC turbine

Subscripts

e	exit
0	dead condition
r	receiver
h	heliostat
i	inlet
j	particular state
su	Sun
ms	molten salt

Greek letters

σ	Boltzmann constant (W/m)
η	Efficiency
δ	Change in property
α	Solar absorbance
ε	Effectiveness

AUTHORSHIP CONTRIBUTIONS

Authors equally contributed to this work.

DATA AVAILABILITY STATEMENT

The authors confirm that the data that supports the findings of this study are available within the article. Raw data that support the finding of this study are available from the corresponding author, upon reasonable request.

CONFLICT OF INTEREST

The authors declared no potential conflicts of interest with respect to the research, authorship, and/or publication of this article.

ETHICS

There are no ethical issues with the publication of this manuscript.

REFERENCES

[1] Praveen RP. Performance analysis and optimization of central receiver solar thermal power plants for utility scale power generation. Sustainability 2020;12:127. [CrossRef]

[2] Khan Y, Mishra RS. Thermo-economic analysis of the combined solar based pre-compression supercritical CO_2 cycle and organic Rankine cycle using ultra low GWP fluids. Therm Sci Eng Prog 2021;23:100925. [CrossRef]

[3] Ahn Y, Bae SJ, Kim M, Cho SK, Baik S, Lee JI, et al. Review of supercritical CO_2 power cycle technology and current status of research and development. Nucl Eng Technol 2015;47:647−661. [CrossRef]

[4] Liang Y, Sun Z, Dong M, Lu J, Yu Z. Investigation of a refrigeration system based on combined supercritical CO_2 power and transcritical CO_2 refrigeration cycles by waste heat recovery of engine. Int J Refrig 2020;118:470−482. [CrossRef]

[5] Al-Sulaiman FA. Exergy analysis of parabolic trough solar collectors integrated with combined steam and organic Rankine cycles. Energy Convers Manag 2014;77:441−449. [CrossRef]

[6] Khatoon S, Kim M. Performance analysis of carbon dioxide based combined power cycle for concentrating solar power. Energy Conversion and Management. 2020;205:112416. [CrossRef]

[7] Song J, Li X, Wang K. Parametric optimization of a combined supercritical CO_2 (sCO_2) cycle and organic Rankine cycle (ORC) system for internal combustion engine (ICE) waste-heat recovery. Energy Convers Manag 2020;218:112999. [CrossRef]

[8] Khan Y, Mishra RS. Performance evaluation of solar based combined pre-compression supercritical CO_2 cycle and organic Rankine cycle. Int J Green Energy 2021;18:172−186. [CrossRef]

[9] Khan Y, Mishra RS. Parametric (exergy-energy) analysis of parabolic trough solar collector-driven combined partial heating supercritical CO_2 cycle and organic Rankine cycle. Energy Sources A Recovery Util Environ Eff 2020. [Preprint). doi: 10.1080/15567036.2020.1788676. [CrossRef]

[10] Singh H, Mishra RS. Performance analysis of solar parabolic trough collectors driven combined supercritical CO_2 and organic Rankine cycle. Eng Sci Technol Int J 2018;21:451−464. [CrossRef]

[11] Yanbolagh DJ, Saraei A, Mazaheri H, Mehrabadi SJ. Exergoeconomic, environmental, economic, and energy-matrices (4E) analysis of three solar distillation systems equipped with condenser and different heaters. J Ther Eng 2021;7:1640−1653. [CrossRef]

[12] Moloney F, Almatrafi E, Goswami DY. Working fluids parametric analysis for the regenerative supercritical organic Rankine cycle for medium geothermal reservoir temperatures, Energy Proc 2017;129:599−606. [CrossRef]

[13] Khan Y, Mishra RS. Performance analysis of solar driven combined recompression main compressor intercooling supercritical CO_2 cycle and organic Rankine cycle using low GWP fluids. Energy Built Environ 2021;3:496−507. [CrossRef]

[14] Khan Y, Mishra RS. Performance comparison of the solar-driven supercritical organic Rankine cycle coupled with the vapour-compression refrigeration cycle. Clean Energy 2021;5:476-491. [CrossRef]

[15] Kose O, Koc Y, Yagli H. Performance improvement of the bottoming steam Rankine cycle (SRC) and organic Rankine cycle (ORC) systems for a triple combined system using gas turbine (GT) as topping cycle. Energy Convers Manag 2020;211:112745. [CrossRef]

[16] Klein SA. Engineering equation solver (EES), Academic Commercial V7.714. 2020 F-Chart Software. Available at: www.fChart.com Last Accessed Date: 26.09.2023.

[17] Padilla RV, Too YCS, Benito R, Stein W. Exergetic analysis of supercritical CO_2 Brayton cycles integrated with solar central receivers. Appl Energy 2015;148:348−365. [CrossRef]

[18] Besarati SM, Goswami DY. Analysis of advanced supercritical carbon dioxide power cycles with a bottoming cycle for concentrating solar power applications. J Sol Energy Eng 2014;136:010904−1.

[19] Ho CK, Iverson BD. Review of high-temperature central receiver designs for concentrating solar power. Renew Sustain Energy Rev 2014;29:835−846. [CrossRef]

[20] Wang X, Liu Q, Lei J, Han W, Jin H. Investigation of thermodynamic performances for two-stage recompression supercritical CO_2 Brayton cycle with high temperature thermal energy storage system. Energy Convers Manag 2018;165:477−487. [CrossRef]

[21] Neises T, Turchi C. A Comparison of supercritical carbon dioxide power cycle configurations with an emphasis on CSP applications. Energy Proced 2014;49:1187−1196. [CrossRef]

[22] Cengel YA, Boles MA. Thermodynamics An Engineering Approach. 5th ed. New York: McGraw-Hill Publication; 2004.

[23] Petela R. Exergy analysis of the solar cylindrical-parabolic cooker. Sol Energy 2005;79:221−233. [CrossRef]

[24] Sukhatme SP, Nayak JK. Solar Energy: Principles of Thermal Collection and Storage, 3rd ed. New Delhi: Tata McGraw-Hill Education; 2008. p. 1−431.

[25] Calm JM. Refrigerant safety. ASHRAE J 1994;36:17−26.

[26] Kulhanek M, Dostal V. Supercritical carbon dioxide cycles thermodynamic analysis and comparison I. Proc. Scco2 Power Cycle Symp, Prague, 2011.

[27] Song J, Li X, Ren X, Gu C. Performance analysis and parametric optimization of supercritical carbon dioxide (sCO_2) cycle with bottoming Organic Rankine Cycle (ORC), Energy 2018;143:406−416. [CrossRef]

[28] Jaszczur M, Hassan Q. An optimisation and sizing of photovoltaic system with supercapacitor for improving self-consumption. Appl Energy 2020;279:115776. [CrossRef]

[29] Sharma A, Rajoria CS, Sing D, Bhamu JP, Kumar R. Numerical simula¬tion of heat transfer characteristics of taper helical and spiral tube heat exchanger. J Ther Eng 2021;7:1591−1603. [CrossRef]

[30] Deshmukh P W, Kasar S V, Sapkal N P. Experimental study of heat transfer in a helical coiled tube biomass fired rotary device. J Ther Eng 2022;8:772−785. [CrossRef]

[31] Ajimotokan H A, Ayuba I, Ibrahim H K. Thermo-economic feasibility analysis of trilateral-cycle power generators for waste heat recovery-to-power applications. J Ther Eng 2022;8:786−797. [CrossRef]